Neural Stem Cell-Mediated Intratumoral Delivery of Gold Nanorods Improves Photothermal Therapy

Rachael Mooney,[*,†] Luella Roma,[†] Donghong Zhao,[†] Desiree Van Haute,[‡] Elizabeth Garcia,[†] Seung U. Kim,[∥] Alexander J. Annala,[†] Karen S. Aboody,[†,§,⊥] and Jacob M. Berlin[*,‡,⊥]

[†]Department of Neurosciences, [‡]Department of Molecular Medicine, and [§]Division of Neurosurgery, Beckman Research Institute at City of Hope, 1500 East Duarte Road, Duarte, California 91010, United States, and [∥]Division of Neurology, Department of Medicine, UBC Hospital, University of British Columbia, Vancouver, British Columbia V6T2B5, Canada. [⊥]Principal Investigators K. Aboody and J. Berlin contributed equally.

ABSTRACT

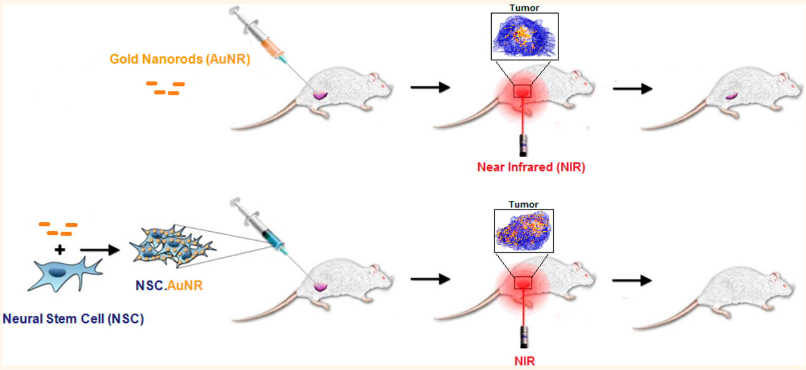

Plasmonic photothermal therapy utilizes biologically inert gold nanorods (AuNRs) as tumor-localized antennas that convert light into heat capable of eliminating cancerous tissue. This approach has lower morbidity than surgical resection and can potentially synergize with other treatment modalities including chemotherapy and immunotherapy. Despite these advantages, it is still challenging to obtain heating of the entire tumor mass while avoiding unnecessary collateral damage to surrounding healthy tissue. It is therefore critical to identify innovative methods to distribute an effective concentration of AuNRs throughout tumors without depositing them in surrounding healthy tissue. Here we demonstrate that AuNR-loaded, tumor-tropic neural stem cells (NSCs) can be used to improve the intratumoral distribution of AuNRs. A simple UV—vis technique for measuring AuNR loading within NSCs was established. It was then confirmed that NSC viability is unimpaired following AuNR loading and that NSCs retain AuNRs long enough to migrate throughout tumors. We then demonstrate that intratumoral injections of AuNR-loaded NSCs are more efficacious than free AuNR injections, as evidenced by reduced recurrence rates of triple-negative breast cancer (MDA-MB-231) xenografts following NIR exposure. Finally, we demonstrate that the distribution of AuNRs throughout the tumors is improved when transported by NSCs, likely resulting in the improved efficacy of AuNR-loaded NSCs as compared to free AuNRs. These findings highlight the advantage of combining cellular therapies and nanotechnology to generate more effective cancer treatments.

KEYWORDS: neural stem cells · gold nanorods · photothermal ablation · tumor tropism

Thermal ablation of tumors is a potentially curative treatment modality that is undergoing rapid technological advancements due to the advent of image-guided procedures and nanotechnology.[1] Tumors exposed to high temperatures undergo coagulation necrosis that results in growth suppression and tumor resorption over the course of several days.[2] This treatment modality is effective against all malignant cells including chemoresistant cells, tumor-initiating cells, and their more differentiated progeny, independent of specific molecular phenotypes.[3] Clinically, percutaneous thermal ablation is now used to treat small, unresectable tumors or patients who are poor surgical candidates.[1] Thermoablative technology offers several practical advantages over surgical resection such as lower morbidity, increased preservation of

* Address correspondence to rmooney@coh.org, jberlin@coh.org.

Received for review September 11, 2014 and accepted November 6, 2014.

10.1021/nn505147w

surrounding tissues, and reduced costs through shorter hospitalization times.[4] Despite these advantages, widespread clinical adoption is still limited because current ablation technologies lack tumor-specific energy absorption.[5] Focused radiofrequency, lasers, and ultrasound all cause diffuse heating. As a result, it is extremely challenging to sufficiently heat tumor margins that often have complex geometries without causing significant damage to surrounding healthy tissue.[5] Incomplete ablation and disease recurrence is common.[6]

Plasmonic photothermal therapy is being developed in an effort to localize heating to tumor tissue.[7] Plasmonic photothermal therapy utilizes biologically inert gold nanoparticles to convert nonharmful laser light into thermal energy. Thus, if the gold nanoparticles can be selectively deposited in tumor tissue, it should be possible to ablate tumors without causing significant collateral damage. In 2003, Hirsch *et al*. demonstrated that injecting ~6.5 μg of pegylated gold silica nanoshells into a 1 cm^3 tumor and exposing it to 810 nm light for 5 min caused intense local heating of 28−60 °C that led to tumor resorption, while exposure of untreated tumors caused heating of only 5−10 °C.[8] Since that initial report, a great deal of effort has gone into developing improved nanomaterials that exhibit increased absorption coefficients and narrowed emission spectra to further amplify tumor-specific heat generation.[9] A number of promising materials have emerged from this work. A recent report compared nanospheres, nanoshells, and nanorods; it was observed that gold nanorods (AuNRs) offer a superior absorption cross-section, and they heat at least 6 times faster than gold-silica nanoshells on a per gram basis.[5] Gold nanomatryoshkas have also shown dramatic enhancement in efficiency over nanoshells.[10] In contrast to this work on new materials, significantly less effort has gone to improving the intratumoral distribution of the gold nanoparticles to obtain more reproducible heating profiles within tumors.[11] As noted above, in the initial report different mice experienced dramatically different amounts of heating in their tumors, from 28 to 60 °C, and this is likely due to the spatial positioning of the gold nanoparticles within the tumor. If the improvements in materials could be coupled with a system that efficiently distributes the nanoparticles throughout the tumor, it would greatly improve the reproducibility of dosing and, by extension, the clinical promise of this therapeutic strategy.

Thus far, the overwhelming majority of AuNP treatments have been given by intravenous or intratumoral injection of free AuNP nanoparticles. AuNP distribution within the tumor has been a function of particle shape and size, vasculature, and behavior of resident immune cells.[5,6] Unfortunately, it is challenging to compare dosing regimens from different laboratories, as very divergent outcomes have been reported even using the same material depending on the tumor model, the AuNP dose administered, and the laser parameters.[10,11] In one case, where a direct comparison was made, it was found that intratumoral injection of AuNPs was more effective than intravenous injection. Following laser treatment, 57% of mice who received intratumoral injections had no tumor reoccurrence, while only 25% of mice receiving intravenous treatment had no tumor recurrence.[12] The improved treatment reproducibility after intratumoral administration is likely due to improved control over the absolute AuNP concentration contained within the tumor, since the accumulated intratumoral AuNP dose 3 days after intravenous administrations can range from 2% to 10% of the injected AuNP dose.[13] While intratumoral administration affords much better dose control, it results in poor intratumoral distribution of the AuNPs, as they generally remain at the site of injection and are unable to further penetrate the tumor mass. The ability of a concentrated AuNP mass to reproducibly generate lethal and irreversible heat injury throughout the entire tumor is limited. There exists a steep negative-temperature gradient from the core toward what are typically uneven tumor margins.[1] Furthermore, the rate of heat dissipation is influenced by unpredictable tumor heterogeneities such as varying degrees of blood perfusion and stromal density.[14] Thus, injecting AuNPs intratumorally solves the dosing problem, but a system to transport the AuNPs throughout the tumor mass is needed.

One emerging approach is to use cells as delivery vehicles that can transport NPs throughout the tumor and along the tumor margin. Many types of tumor-tropic cells can be used to improve NP delivery within tumors, including mesenchymal stem cells,[15] macrophages,[16] and T-cells.[17] Of particular note for improving plasmonic photothermal therapy, Choi *et al*. demonstrated that gold nanoshells endocytosed by macrophages still heat when exposed to NIR light and the loaded cells can infiltrate tumor spheroids.[18] This result was independently validated by Madsen *et al*.[16] When tested in a mouse model, these cells can also migrate to brain tumors.[19] We chose to focus on the use of the established tumor-tropic HB1.F3.CD immortalized neural stem cell (NSC) line. These cells are nontumorigenic and minimally immunogenic and have shown promise in targeting therapy to tumors in preclinical brain and breast cancer models.[20,21] They have also been manufactured as a clinical grade master cell bank and used in a first-in-human safety study.[20] We have previously demonstrated that NSCs can overcome biological barriers, such as dense tumor stroma and hypoxic tumor cores,[22] to improve the distribution of therapeutic genes,[20] antibodies,[23] and oncolytic viruses.[24−26] Recently, we have shown that following intratumoral administration, NPs transported by these

NSCs have dramatically enhanced tumor coverage as compared to NPs alone, and this leads to improved drug delivery.[27−29] To take advantage of this property for plasmonic photothermal therapy, we also demonstrated that following endocytosis of AuNRS, NSCs have no impairment of their viability or tropism *in vitro*.[30] We further demonstrated that a single NSC.AuNR conjugate is capable of generating enough heat when exposed to NIR light to kill 50 triple-negative breast cancer (TNBC) cells *in vitro*, and in a very small pilot experiment the NSC.AuNRs appeared to perform better than free AuNRs alone for treating a xenograft mouse model of TNBC.[30] TNBC was chosen for our initial studies because it is an attractive candidate for plasmonic photothermal therapy given that it is characterized by tumors that do not express estrogen, progesterone, or HER-2 receptors, making it unsuitable for treatment with modern targeted therapies, and has a worse clinical outcome than other breast cancer subtypes.[31] Furthermore, we have demonstrated that NSCs exhibit a strong tropic response toward TNBC lines.[21]

In the present work, we demonstrate that NSC.AuNR conjugates can be used to improve the intratumoral distribution of AuNRs and thereby increase the efficacy of plasmonic photothermal therapy. We first established a spectrophotometric AuNR quantification assay that enables rapid and simple measurement of AuNR content within free AuNR and NSC.AuNR treatments. We next established thermal dosing conditions (laser duration, power, and AuNR concentration) that are sufficient to induce the initial resorption of most treated xenograft tumors established in the flank of mice. These variables were then held constant when comparing the incidence of tumor recurrence following intratumoral treatment with either free AuNRs or NSC.AuNRs and subsequent exposure to NIR. The mice treated with NSC.AuNRs had a statistically significant lower rate of recurrence then those treated with free AuNRs. When the intratumoral distribution of AuNRs was assessed, the NSC.AuNRs had a remarkably broader and more even distribution throughout the tumor as compared to the free AuNRs. While this effect is significant in small tumors in mice, it may be even more profound in larger tumors found in humans. Future testing will evaluate this potential and determine the clinical potential of this therapy.

RESULTS

Spectrophotometric AuNR Quantification. It was first necessary to develop a quantitative technique that would allow comparison of cellular AuNR content with that of free AuNR solutions. The concentration of experimental AuNR samples is commonly determined using spectrophotometric methods that compare the optical density measured in each sample against a standard curve. To measure intracellular metal content, however, inductively coupled mass spectrometry (ICP-MS) is the "gold standard" technique commonly used because cellular debris will not interfere with metal quantifications and it is sensitive enough to detect metal contents in the 1 ppb range (~0.1 μg/mL).[32] We previously demonstrated that NSCs robustly internalize 11-mercaptoundecyltrimethylammonium bromide (MUTAB)-conjugated AuNRs without inducing NSC toxicity (Figure 1a) and used ICP-MS to determine that the AuNR content within 1×10^6 NSCs after a 16 h incubation with a solution of 5×10^{12} AuNRs/mL is approximately 1.5 μg of Au.[30] We have since discovered that this level of uptake varies with each commercially obtained AuNR batch, and the resulting AuNR content can range from 1.5 to 42 μg of Au per 1×10^6 NSCs (Supplementary Figure 1). This variability in AuNR loading mandated that the AuNR content within NSCs be quantified before each *in vivo* experiment. However, there are practical limitations of using ICP-MS to quantify cellular AuNR content immediately prior to *in vivo* experiments including the need to digest for hours in strong acid to liberate the Au ions and the requirement for specialized equipment that is not readily available in most institutions. Thus, we developed a simple and rapid spectrophotometric AuNR quantification protocol that can be used prior to each *in vivo* experiment to equalize the AuNR dose administered in both free AuNR and NSC.AuNR injections.

First, the dynamic range of the spectrophotometric assay was determined by measuring the absorbance at 810 nm for a series of serial dilutions of AuNR standards (Supplementary Figure 2a). As expected, the limit of detection using optical density measurements (25 μg/mL) was 2 orders of magnitude less sensitive than ICP-MS, but this limit of detection still rendered the assay useful, as the concentration of AuNR uptake by NSCs is typically high enough to generate detectable optical density increases when sampling a moderately low number of NSCs (1×10^5). The standard curve was linear between 80 and 405 μg/mL (Supplementary Figure 2b). Next, we evaluated if NSCs (following lysis) would interfere with the accuracy of AuNR quantification by doping AuNR standards with 1×10^5 NSCs lysed in diH_2O. No significant difference was observed for the absorption of free AuNRs or AuNRs at the same concentration mixed with lysed NSCs (Figure 1b). In addition, we compared the full absorbance spectra from 200 to 1000 nm for both free AuNRs and for NSC.AuNRs lysed in diH_2O. There was no difference between the samples, with both samples revealing two absorption peaks (a small peak at 520 nm and a larger peak at 810 nm) that respectively correspond to the short and long AuNR axis (Figure 1c). Finally, we demonstrated that the amount of internalized AuNRs measured by absorbance at 810 nm is highly correlated with that measured by ICP-MS

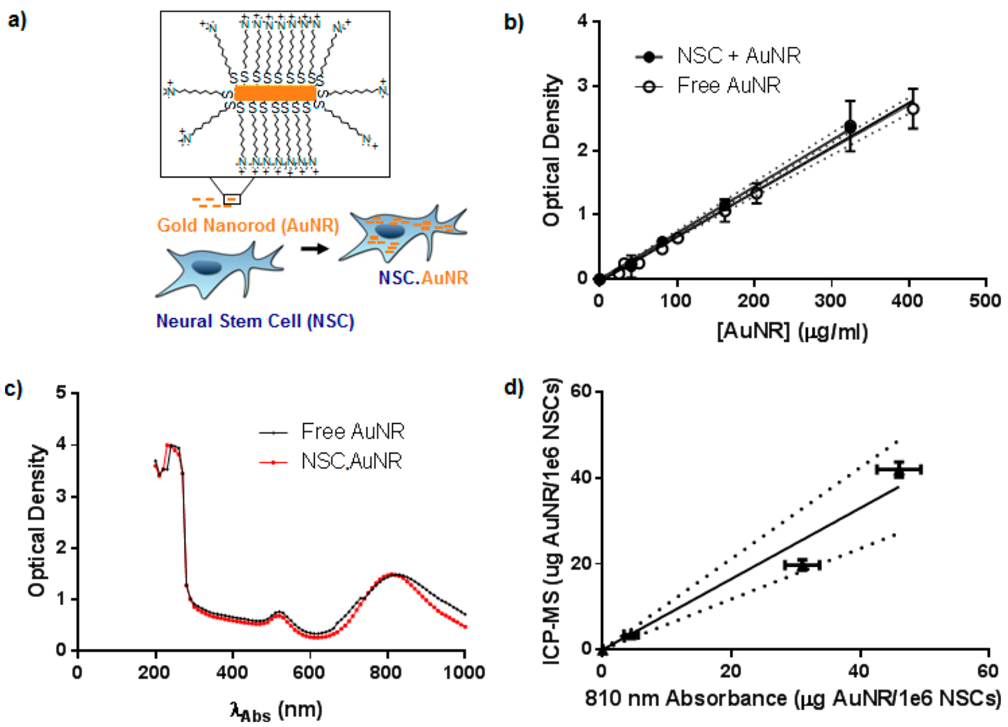

Figure 1. Spectrophotometric quantification of AuNR content within NSCs. (a) Schematic depicting MUTAB-conjugated AuNR uptake by NSCs. (b) Dynamic range of spectrophotmetric assay using abs = 810 nm with (closed circles) and without (open circles) the addition of 1 × 10^5 unlabled NSCs lysed in diH$_2$O (dashed line = 95% confidence intervals). Error bars represent one standard deviation. (c) Spectral analysis of a 320 μg/mL AuNR solution generated using free AuNRs (black) or NSC.AuNRs (red) lysed in diH$_2$O. (d) Results over a range of intracellular gold content demonstrate a linear correlation (slope = 0.8262 ± 0.074 05; CI 0.7961 to 0.9999, R^2 = 0.9539) for measurements obtained using ICP-MS *versus* spectroscopy.

(Figure 1d). While inaccuracies can be introduced by inadequate lysis of the cell product, these data confirm that time-efficient, inexpensive spectrophotometric measurements (λ_{abs} = 810 nm) can be used in place of ICP-MS to ensure comparable AuNR content is present between the free AuNR and NSC.AuNR samples prior to *in vivo* injections.

Time Course of AuNR Uptake and Release by NSCs. Having established a spectrophotometric protocol, it was used to assess the time course over which AuNRs are taken up and retained within NSCs. This information is needed to ensure that NSCs remain efficiently loaded for at least 3 days while they actively distribute AuNRs throughout the tumor interstitium.[33] To monitor AuNR uptake kinetics, NSCs were incubated for increasing durations with a solution of 5 × 10^{12} AuNRs/mL. Figure 2a shows that AuNR uptake significantly increases for the first 2−4 h and then gradually slows and reaches a plateau at 8−16 h. The time scale and uptake pattern are in agreement with previous work[34,35] and exhibit the saturation characteristics of receptor-mediated endocytosis.[34] Together these results confirmed that a 16 h incubation period is sufficient to achieve maximum AuNR loading into NSCs. The maximum uptake observed with any AuNR batch was 42 μg of Au per 1 × 10^6 NSCs. Because this is an order of magnitude greater uptake than we previously reported, we confirmed the ability of these AuNR-loaded NSCs to migrate toward tumor-specific signals *in vitro* (Figure 2b).

It has been reported that internalized AuNRs are eventually eliminated from cells—primarily during mitotic divisions but also *via* exocytosis—with the release rate increasing exponentially over time.[36] Thus, it was also essential to confirm that AuNR-loaded NSCs retain therapeutically relevant AuNR levels after a 3-day period. While it was found that AuNR content does indeed decrease exponentially over time (right axis, Figure 2c) as the NSCs proliferate (DNA content, left axis, Figure 2c), the amount of AuNRs remaining on day 3 was sufficient for the NSC.AuNRs to generate cyto-ablative heat upon exposure to 810 nm light (Figure 2d,e). Furthermore, we suspect that the observed release of AuNRs from HB1.F3 NSCs *in vitro* overestimates that which would occur upon transplantation *in vivo* where NSCs cease division by 48−72 h.[20] Together these data suggest that AuNR-loaded NSCs are capable of retaining therapeutic AuNR levels for 3 days.

Optimizing Tumor Model, Laser Power, and AuNR Dose. Before assessing the performance of NSC.AuNRs *in vivo*, we needed to establish the tumor model, laser settings, and AuNR concentration that would be used. The vast majority of AuNR-based photothermal ablation studies utilize subcutaneous tumor models established in the flank. Because we are interested in developing

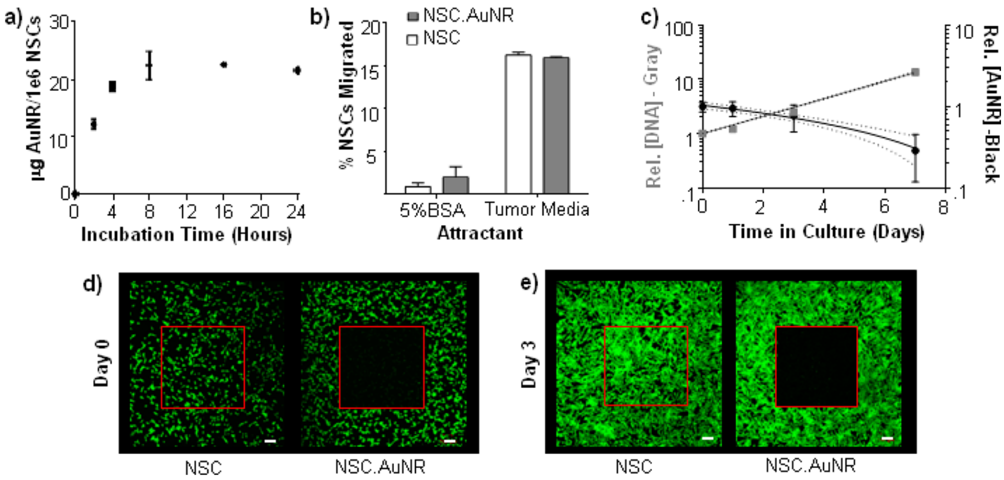

Figure 2. AuNR loading optimization. (a) Spectrophotometric analysis of AuNR uptake in NSCs after incubating in a concentrated AuNR solution for increasing time periods. (b) Relative tumor tropisms of untreated and AuNR-treated NSCs (22 μg AuNR/1 × 10^6 NSCs) were compared in an *in vitro* Transwell Boyden migration assay. Bovine serum albumin (BSA, 5%) was used as a negative control. (c) HB1.F3.CD cells were treated with AuNRs for 16 h, replated, and collected at different time points. Spectrophotometric (black) and fluorimetric DNA quantification (gray) assays were respectively used to monitor AuNP retention and NSC number within cultures grown for 1 week *in vitro*. As culture time increases, AuNR content decreases at an exponential rate with a slope of -2.321 ± 0.1861 (CI -3.122 to -1.521, $R^2 = 0.9873$). A Runs test confirms that the observed departure from linearity on day 7 is not significant ($p = 0.667$). Dotted lines represent 95% confidence intervals. (d, e) HB1.F3.CD neural stem cells were incubated with AuNRs on day 0 (44 μg AuNR/1 × 10^6 NSCs) and then either immediately (d) or after 3 days of culture (e) exposed to a $\lambda = 810$ nm NIR laser using a 10× objective. Representative 5× images are shown after laser exposure of both untreated and AuNR-treated NSCs; the area exposed to the laser using the 10× objective is shown with a red box. Scale bar = 100 μm.

this therapy for triple-negative breast cancer applications, we also explored the possibility of using an orthotopic tumor model established in the mammary gland fat pad. First, either the flank or the mammary gland fat pad in tumor-free nude female mice was exposed to an NIR laser regimen (2 W/cm^2, 5 min) that was reported to have negligible absorption by skin covering the flank.[2] We observed that while this laser exposure had no damaging effects on flank tissue (Figure 3a), there was an immediate inflammatory reaction to this laser power when applied to the skin covering the mammary gland fat pad even in the absence of gold (Figure 3b). Due to the increased sensitivity of the mammary tissue, we opted to utilize the standard flank model for our studies.

We next determined an AuNR dose sufficient to induce tumor ablation without rapid recurrence. This was necessary because there are only a few studies reported to date using plasmonic photothermal therapy after an intratumoral injection, and no consensus exists regarding the gold content needed to reproducibly resorb a tumor of a given tumor size. MDA.MB.231.Ffluc human TNBC cells modified to express the reporter gene Ffluc were injected into the flanks of nude mice. After 14 days, mice with tumors 5−7 mm in diameter were randomly assigned to be injected with either 0, 1.25, 6.25, 12.5, or 25 μg of AuNR. Xenogen imaging was used to monitor tumor resorption and recurrence over the next 2 weeks. Intratumoral administrations of increasing AuNR doses were delivered; then tumors were exposed to NIR irradiation 3 days later. Our goal was to give treatment such that, in animals treated with free AuNRs, the AuNRs would still be in the tumor, while, for animals treated with NSC.AuNRs, the NSCs would have time to migrate from the injection point throughout the tumor. Treatment after 3 days was chosen based on a previous report that showed, following intratumoral injections, AuNR dose within the tumor remains unchanged over a period of 2−4 days.[37] Following treatment, the results show that the Ffluc tumor signal decreased immediately following tumor ablation at every tested AuNR concentration (Figure 3c). However, only at AuNR doses of 12.5 μg and above was sustained tumor elimination observed. Because sustained tumor elimination was observed with 12.5 μg of AuNR and this dose was associated with less damage to surrounding normal tissue than occurred using 25 μg of AuNR, a AuNR dose of 12.5 μg was used for future experiments.

NSC-Mediated Improvement in Intratumoral AuNR Photothermal Ablation. To test whether NSC-mediated delivery of AuNRs can improve the efficacy of photothermal tumor ablation, we established MDA-MB-231.Ffluc tumors in the flank of 23 mice (2 separate experiments: 15 mice in experiment 1, and 8 mice in experiment 2). Two weeks after tumor engraftment the mice were randomized into three treatment groups. Each group received intratumoral injections of either phosphate-buffered saline (PBS), free AuNRs (12.5 μg), or NSC.AuNRs (12.5 μg of AuNR in 1 × 10^5 NSCs). After 72 h, mice were anesthetized and all tumors were exposed to an 810 nm NIR laser at a power of 2 W/cm^2 for 5 min.

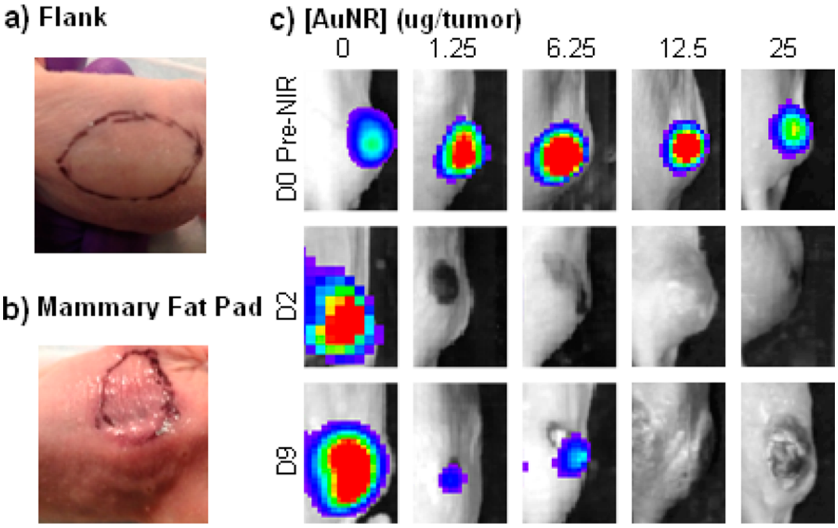

Figure 3. AuNR dose establishment. (a, b) Photographs showing nude mice skin sensitivity immediately after exposure to NIR laser in either the (a) flank or (b) mammary gland fat pad. (c) MDA-MB-231.Ffluc cancer cells were injected into the flank of nude mice. Mice were Xenogen imaged using luciferin substrate pre- and post-NIR exposure. Signals from primary breast tumors before (top panel) NIR exposure and 2 days (middle panel) and 9 days (bottom panel) after NIR laser exposure are shown.

For experiment 1, there were three equal groups of 5 mice. As described below, we found that for mice receiving therapy there were two distinct groups, "partial responders" and "complete responders", that resulted from the mechanics of the initial injection. To obtain a sufficient number of "complete responders" for statistical analysis, the experiment was repeated in experiment 2 with 2 control mice, 4 mice receiving free AuNRs, and 4 mice receiving NSC.AuNRs. Unfortunately, 2 of the mice from the free AuNRs group became ill independent of treatment and had to be excluded. Thus, the final group sizing was 7 control mice, 7 treated with free AuNRs, and 9 treated with NSC.AuNRs, which provided sufficient numbers for statistical analysis.

We observed significant heterogeneity in the initial injection of both the free AuNR and NSC.AuNR treatment groups. Neither the NSC.AuNR suspensions nor the free AuNR suspensions easily infused into the dense tumor matrix and instead usually flowed over to one side of the tumor. In some cases, the material flowed such that following injection it settled predominantly outside of the tumor mass. As a result, approximately 1/3 of the tumors exposed to NIR in both free AuNR and NSC.AuNR treatment groups did not completely resorb, as evidenced by a positive Xenogen signal 2 days after treatment ($n = 3$ of 9 for NSC.AuNR; $n = 2$ of 7 for AuNR) (Figure 4a–c). This initial tumor resorption rate is similar to that reported by others using intratumoral AuNR injections.[2] Thus, there are two separate problems with the intratumoral injections of free AuNR injections that need to be addressed. The first is the initial injection parameters that result in unpredictable AuNR distributions dictated by pressure gradients and matrix constraints that exist within these very stiff tumors. In the mice that did not fully respond initially, the AuNR solutions were largely pushed outside of the tumor proper and accumulated at one location along the tumor perimeter. Thus, the AuNR dose inside the tumor is unknown. NSC-mediated AuNR delivery does not appear to overcome this problem; future studies will focus on improving material deposition at the tumor site, perhaps by using slow infusions.

The second problem is the efficacy of AuNRs that are deposited in the tumor. To isolate this problem for analysis and evaluate the impact of NSCs on intratumoral distribution of AuNRs and the subsequent photothermal ablation, we considered only mice whose tumors completely resorbed, as this meant we could be sure we were comparing mice that received comparable AuNR doses. In each treatment group (free AuNRs and NSC.AuNRs), 5 mice had complete tumor ablation, as indicated by no Ffluc signal on day 2 and a tumor volume measurement of 0 mm^3 after a single laser exposure. In these mice, the time to tumor recurrence and long-term survival were monitored over the next 100 days. Mice were euthanized upon reaching clinical symptoms and/or the size of the recurrent tumor grew to exceed 1.5 cm^3. The resulting Kaplan–Meir plot demonstrates significantly improved overall survival when AuNRs were delivered within NSCs as compared to free AuNR suspensions (p value = 0.0438 using a Gehan–Breslow–Wilcoxon test) (Figure 4d). This was the result of reduced tumor recurrence in the NSC.AuNR-treated group. As for the animals that experienced tumor recurrence (defined as a positive Xenogen signal during weekly imaging), the median time to recurrence was about 21 days in both the NSC.AuNR- and free AuNR-treated animals ($p = 0.502$). The growth rate of recurrent tumors was no different

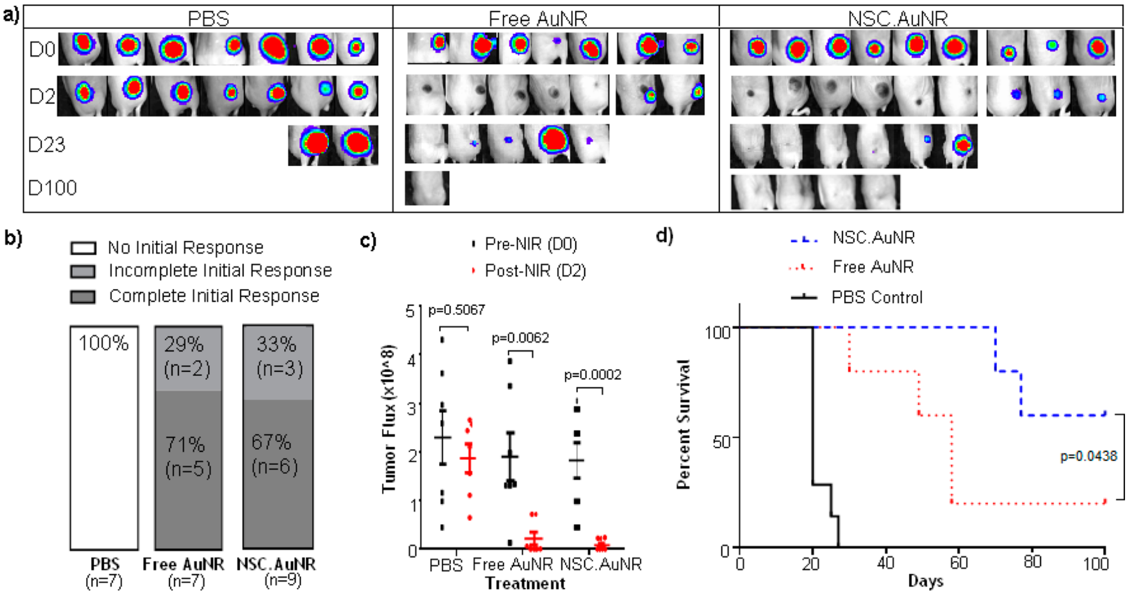

Figure 4. NSC.AuNRs reduce tumor recurrence post-NIR-laser treatment. (a) Time course Xenogen images demonstrating MDA-MB-231.ffluc tumor resorption and recurrence in female nude mice after direct injection of either PBS, free AuNRs (12.5 μg), or NSC.AuNRs (12.5 μg of AuNR in 1 × 10^5 NSCs) and a single NIR exposure (5 min, 2 W/cm^2, 5 mm diameter). Day 0 images represent pre-NIR flux levels. (b) Cumulative results demonstrating the percentage of tumors that resorbed after a single NIR exposure. (c) Quantitative representation of luminescent flux signal before (day 0) and after (day 2) NIR exposure. Error bars represent the standard error of the mean. (d) Kaplan–Meier survival curve demonstrating long-term survival of mice that received either PBS, free AuNR, or NSC.AuNRs prior to NIR laser exposure. Only mice that experienced complete tumor elimination following AuNR+NIR or NSC.AuNR+NIR treatment are included.

than that of the original tumor and resulted in animal euthanasia within 2–3 weeks in both treatment groups. However, 3 of the 5 mice that received NSC.AuNRs remained tumor free until the end of the 100-day study. In contrast, only 1 mouse treated with free AuNRs remained tumor free (Figure 4a,d).

NSC-Mediated Improvements in Intratumoral AuNR Distribution. We hypothesized that the reduction in tumor recurrence observed when mice are treated with NSC.AuNRs rather than free AuNRs is attributable to more even AuNR biodistribution throughout the tumor. Therefore, we performed a proof-of-principle biodistribution study to determine if NSCs could alter the *in vivo* distribution of AuNRs. Two nude adult female mice were implanted with MDA.MB.231.Ffluc human TNBC cells in the right flank and then 2 weeks later injected intratumorally with either free AuNR suspensions (12.5 μg) or NSC.AuNRs (12.5 μg in ~1 × 10^5 NSCs). Three days after injection, the tumors were harvested and sections were obtained at 150 μm intervals. Dark-field images were acquired using a 10× objective for all sections, then tiled to generate an image displaying the AuNR distribution in the entire $x-y$ tumor plane (Figure 5a,b). ImagePro Premier software was used to flatten light fluctuations across the mapped image. Reconstruct software was then used to align the tissue slices and automate AuNR recognition. Five pixels in AuNR-rich regions and five control pixels were used to establish hue, saturation, and intensity thresholds. Any continuous pixels that were above these thresholds were assigned as AuNRs and are pseudocolored red (Figure 5c,d). The tumor perimeter was traced by hand. Reconstruct software utilized these AuNR (red) and tumor boundary (blue) traces to generate a 3D rendering of AuNR distribution within each tumor (Figure 5e,f).

The results demonstrate that although the gold distribution after free AuNR injections remains localized near the central core of the tumor (Figure 5a,c,e), the gold distribution after NSC.AuNR injections is more evenly distributed (Figure 5b,d,f). This distribution pattern observed after free AuNR injections is consistent with a previous report that characterized intratumoral AuNR distribution using X-ray CT,[5] in which a concentration of AuNRs was observed solely in the middle of the tumor. It is known from microwave ablation studies that a single large heat source is an inefficient means of delivering energy to a large volume of tissue.[34] Much of the energy generated by very high core temperatures is "wasted" on tissue that is already necrotic because thermal conduction is largely mitigated by tissue perfusion.[35] Thus, spatially distributing the AuNR heat generation by delivering them within NSCs may create a more uniform thermal profile and increase the likelihood that cytotoxic temperatures are reached at all points within the tumor.

CONCLUSIONS

One of the greatest challenges of translating plasmonic photothermal ablation into the clinic is optimizing *in vivo* AuNR delivery. Direct intratumoral injections can be used to circumvent inefficiencies and off-target

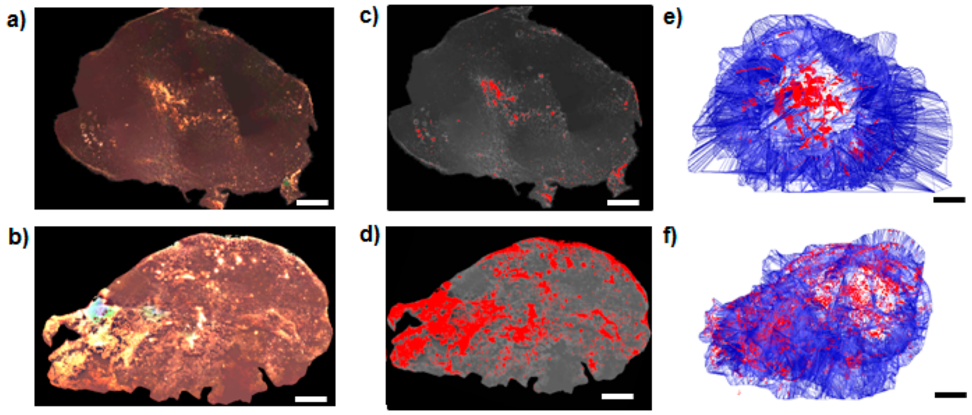

Figure 5. Comparison of free AuNR and NSC.AuNR distribution after intratumoral injection. Three days after AuNR injection, tumors were sectioned. Every 150 μm, sections were imaged using dark-field microscopy. (a, b) Tiled, flattened, dark-field micrographs of entire cross sections of tumors injected with free AuNRs (a) or NSC.AuNRs (b). AuNRs are visible as dense, bright gold signals. (c, d) Mapped cross sections of tumors injected with free AuNRs (c) or NSC.AuNRs (d). (e, f) 3D projection of all mapped AuNR (red) and tumor (blue) traces generated using Reconstruct software in tumors that received free AuNR (e) or NSC.AuNR (f). Scale bar = 1 mm and applies to all images.

deposition observed after intravenous administration, but achieving a homogeneous AuNR distribution within the tumor is still a difficult hurdle to overcome. In this study, we demonstrate that intratumoral NSC-mediated AuNR delivery results in a more homogeneous AuNR distribution within the tumor. The improved distribution translates to reduced tumor recurrence rates after NIR exposure for the NSC.AuNR-treated group as compared to the free AuNR-treated group. In the future, this approach could be further enhanced by methods that improve the efficiency and accuracy of intratumoral injections. Beyond improved distribution, there are other potential advantages inherent in this paradigm. The tumor-tropic cells themselves could be engineered to carry other complementary therapeutics that would enhance the effect of thermal ablation. Together these findings highlight the advantage of combining cellular therapies and nanotechnology to generate more effective cancer treatments. While intratumoral injection is likely the preferred route of administration for plasmonic photothermal ablation due to the ability to directly control total gold dose in the tumor, it is possible that in the future the improved intratumoral distribution of NSCs could be applied to intravenous administration of other NP therapeutics. We have previously demonstrated that NSCs exhibit tumor-specific tropism following intravenous administration[22,23] and demonstrated that, following intravenous injection, NSCs can transport surface-bound NPs across the blood brain barrier.[29] Intravenous applications will particularly benefit from continued optimization of dosing regimen and NSC survival and tumor tropism following injection. Many of these challenges are avoided for intratumoral administration for plasmonic photothermal ablation, which may accelerate completion of preclinical studies using the NSC.AuNRs.

MATERIALS AND METHODS

Cell Culture. All cell lines were cultured in Dulbecco's modified Eagle's medium (DMEM) (Invitrogen) supplemented with 10% fetal bovine serum (Gemini Bio), 1% L-glutamine (Invitrogen), and 1% penicillin–streptomycin (Invitrogen) and maintained at 37 °C in a humidified incubator (Thermo Electron Corporation) containing 6% CO_2. When cells reached 80% confluency, they were passaged using a 0.05% trypsin/EDTA solution (Invitrogen); media was changed every 2 or 3 days. The firefly luciferase (Fluc)-expressing TNBC cell line MDA-MB-231.Ffluc was obtained from American Type Culture Collection. MDA-MB-231.Ffluc cells were used to generate tumor cell-conditioned media by replacing culture media with serum-free media when cells were 80% confluent, followed by a 48 h incubation. Neural stem cell line: The human, v-*myc* immortalized, HB1.F3 NSC line was obtained from Dr. Seung Kim (University of British Columbia).

Preparation of MUTAB-Coated AuNR Solutions. 11-Mercaptoundecyltrimethylammonnium bromide-coated gold nanorods with 40 nm × 10 nm dimensions and longitudinal plasmon resonances at 810 nm were supplied by Nanopartz, a division of Concurrent Analytical, Inc. The samples were maintained in deionized (DI) water at 4 °C at a concentration of 36.1 mg/mL prior to serial dilutions or application to NSCs. AuNRs were then centrifuged at 14 000 rpm, 0 °C, for 15 min and gently resuspended into either DI water for OD readings or the appropriate volume of fetal bovine serum containing DMEM for NSC loading.

Inductively Coupled Mass Spectrometry AuNR Quantification. NSCs were incubated with AuNRs (5×10^{12} AuNRs/mL) for 16 h. AuNR-loaded NSCs were carefully washed with PBS buffer (1×) three times to remove unloaded AuNR. A 1 mL amount of BDH Aristar Plus Nitric Acid (70%) was used to digest the cell pellet, and the sample was diluted to 5 mL with 2% HNO_3. Gold concentration was determined by ICP-MS analysis on a Thermo X-Series 2 using a concentric nebulizer, impact bead spray chamber, and torch with a fixed quartz injector. An Xt interface was used. Plasma power was 1250 W, nebulizer flow was 0.82 L/min, cool gas flow was 14 L/min, and auxiliary gas flow was 1.1 L/min. Sample flow to the nebulizer was approximately 400 μL/min. A standard curve was made using serial dilutions of a 1 ppm solution of gold standard solution (Spex CertiPrep). Data were analyzed quantitatively in a spreadsheet program.

Spectrophotometric AuNR Quantification. *Standard curve generation*: Serial dilutions of a stock AuNR solution (5×10^{13} AuNRs/mL) with or without 1 × 10^5 lysed NSCs added were aliquoted in triplicate wells of a clear flat-bottom plate. Deionized water was used as a blank that was subtracted from all absorbance values. A spectral reading (λ = 810 nm) was performed on the samples using a SpectraMax M3 microplate reader (Molecular Devices, CA, USA). *AuNR uptake kinetics*: AuNR solutions (5 × 10^{12} AuNRs/mL NSC culture media) were incubated with NSCs for 2, 4, 8, 16, or 24 h. At each time point, NSC.AuNR conjugates were trypsinized, centrifuged at 1200 rpm for 5 min, and rinsed with PBS twice, and an aliquot was manually counted *via* hematocytometer and trypan blue. A spectral reading (λ = 810 nm) on 1 × 10^5 cells was then performed. *AuNR release kinetics*: NSCs were incubated with 5 × 10^{12} AuNRs/mL for 16 h. At select time points (day 0, day 1, day 3, and day 7), NSC.AuNR conjugates were trypsinized, centrifuged at 1200 rpm for 5 min, and rinsed with PBS twice, and an aliquot was manually counted *via* hematocytometer and trypan blue. A spectral reading (λ = 810 nm) on 1 × 10^5 cells was then performed.

***In Vitro* Photothermal Ablation of AuNR-Loaded NSCs.** NSCs were incubated with 5 × 10^{12} AuNRs/mL for 16 h, after which the NSCs were rinsed and replated. On either day 0 or day 3, AuNR-loaded NSCs were exposed to laser light using a Zeiss LSM 510 two-photon inverted confocal microscope and 10× objective at 810 nm and 2000 mW using a pulse sequence in which each pixel was exposed for 1.6 μs one hundred times; as a result of the number of pixels exposed, there was a delay of 1.7 s between each exposure for an individual pixel. Thus, each area of the square was exposed for a total of 160 μs during a total scan time of approximately 3 min. A targeted region was heated in each condition using a 10× objective. Postheating, laser-treated and nontreated NSCs were stained with calcein AM LIVE solution and imaged with a 5× objective to clearly visualize the targeted region.

***In Vitro* Transwell Boyden Migration Assay.** As previously described,[30] in a 24-well tissue culture plate 500 μL of target media (either containing BSA as a negative control or derived from the culture of MDA-MB-231.Ffluc breast cancer cells) was added to each well. At a density of 1 × 10^5 cells/well, control and AuNR-loaded NSCs in DMEM and 5% w/v BSA were placed in the upper Transwell chambers and incubated at 37 °C for 4 h. After the incubation period, in order to quantify the cells that had migrated to the bottom side of the membrane, the Transwell chambers were placed in a new 24-well tissue culture plate containing accutase and incubated 10 min at 37 °C. Detached cells were then transferred to a 96-well V-bottom plate, centrifuged at 1500 rpm for 5 min, and resuspended in cell lysis buffer. The PicoGreen (Invitrogen) DNA quantification assay was used according to the manufacturer's instructions to determine the number of migrated cells.

Establishment of Xenograft Tumors. Female, athymic nude mice 6−8 weeks of age (Charles River) were maintained under specific pathogen-free conditions at the City of Hope Animal Resource Center, and all procedures were reviewed and approved by the City of Hope Animal Care Committee. Intramammary fat pad and flank xenografts required anesthetizing the mice by isoflurane (1.5 L/oxygen, 4% isoflurane). MDA-MB-231.Ffluc tumor cells (5 × 10^6) were suspended in Matrigel prior to injections. Tumor volumes were measured using a caliper (±0.1) every week, and tumor volume was calculated by $\text{mm}^3 = L \times W^2/2$, where L is the longest dimension and W is measured perpendicular to L. After 14 days, mice were selected for treatment if the subcutaneous tumors reached 5−7 mm diameter as measured with a digital caliper. Selected mice were anesthetized with isoflurane before 10 μL intratumoral injections of either PBS, free AuNRs (12.5 μg), or NSC.AuNRs (12.5 μg within ~1 × 10^5 NSCs). Three days later, mice were either exposed to NIR laser or harvested for biodistribution assessments.

***In Vivo* Photothermal Therapy.** Three days post-intratumoral injection mice were anesthesized with a cocktail of ketamine and xylazine. Lubricant ointment was applied to mice eyes to prevent drying. Glycerin was applied to the flank before laser application, and the eyes were covered with a black felt cover to protect them from the laser. A continuous-watt laser (811 nm, 2 W/cm^2, RPMC Lasers, Inc., O'Fallon, MO, USA) was applied to the right flank for 5 min. Silver sulfadizine 1% cream was applied to the focal tumor immediately after laser treatment. Once mice recovered from the anesthesia, Buprenex was subcutaneously injected for pain management. Xenogen imaging was performed 2 days later and then weekly to monitor changes in tumor burden in each animal.

Xenogen Imaging. Firefly luciferase expressing tumor cells were imaged in mice using a charge-coupled device camera (Xenogen IVIS-100) coupled to the Living Image acquisition and analysis software. Mice received an intraperitoneal injection of D-luciferin substrate suspended in PBS at 4.29 mg/mouse. Images were captured while the mice were anesthetized by isoflurane (1.5 L/oxygen, 4% isoflurane) and kept in an induction chamber. Light emission was measured over an integration time of 10 s at 18 min after injection of luciferin.

Intratumoral AuNR Biodistribution. Tumors harvested for biodistribution analysis were fixed in 4% paraformaldehye for 48 h (pH = 7.4) prior to sinking in 30% sucrose. The tumors were frozen in Tissue Tek OCT (Sakura Finetek USA) and sectioned on a Leica CM1510 S cryostat (Leica Biosystems). Sections (10 μm thick) were collected on positively charged slides (Thermo Fisher Scientific, cat. no. 12-550-15) for dark-field imaging. Every 15th section was imaged using a dark-field microscope system (Cytoviva Inc.). Image-Pro Plus 3.0 software (Media Cybernetics; Silver Spring, MD, USA) was then used to tile and preprocess the images to flatten light fluctuations. Finally, open source Reconstruct software[36] (Boston University) was used to automatically detect AuNR presence based on saturation, color, and intensity thresholds established using five pixels in AuNR-rich regions and five control pixels. Any continuous pixels that were above these thresholds were assigned as AuNRs. Tumor perimeters were traced by hand,; then AuNR and tumor traces were used to construct 3D projections of AuNR distribution within the tumor.

Statistical Analysis. Data are presented as mean ± SEM unless otherwise stated. Statistical significance was determined using a two-tailed Student's *t* test ($*p < 0.05$) unless otherwise stated.

Conflict of Interest: The authors declare the following competing financial interest(s): K.S.A. and A.J.A. are officers and board members of TheraBiologics, Inc., a clinical stage biopharmaceutical company supporting development of NSC-mediated cancer treatments. The remaining authors declare no conflict of interest.

Acknowledgment. We gratefully acknowledge ICP-MS instrumentation under the supervision of Nathan Dalleska at the Environmental Analysis Center at the California Institute of Technology, and Dr. Brian Armstrong for his assistance with *in vitro* thermal ablation experiments. Studies were supported by generous funding from STOP Cancer, The Rosalinde and Arthur Gilbert Foundation, Mary Kay Foundation, California Institute of Regenerative Medicine, and the Alvarez Family Foundation. R.M. was supported by a fellowship from the California Institute for Regenerative Medicine (CIRM, grant no. TG2-01150) and the Ladies Auxiliary of the Veterans of Foreign Wars. L.R. was supported by the CIRM Bridges Training Program (grant no. TB1-01177). Materials transfer information is available from the City of Hope Office of Technology Licensing (http://www.cityofhope.org/research/support/center-for-applied-technology-development/office-of-technology-licensing/Pages/default.aspx). Research reported in this publication included work performed in the Light Microscopy Digital Imaging and Animal Resource Center Cores supported by the National Cancer Institute of the National Institutes of Health under award no. P30CA33572. The contents of this publication are solely the responsibility of the authors and do not necessarily represent the official views of the National Institutes of Health, CIRM, or any other agency of the State of California.

Supporting Information Available: A description of supplementary methods and figures demonstrating variable AuNR uptake by NSCs with different AuNR batches (Supplementary Figure 1) and the linear range for the AuNR spectrophotometric assay (Supplementary Figure 2). These materials are available free of charge *via* the Internet at http://pubs.acs.org.

REFERENCES AND NOTES

1. Chu, K. F.; Dupuy, D. E. Thermal Ablation of Tumours: Biological Mechanisms and Advances in Therapy. *Nat. Rev. Cancer* **2014**, *14*, 199–208.
2. Dickerson, E. B.; Dreaden, E. C.; Huang, X.; El-Sayed, I. H.; Chu, H.; Pushpanketh, S.; McDonald, J. F.; El-Sayed, M. A. Gold Nanorod Assisted near-Infrared Plasmonic Photothermal Therapy (Pptt) of Squamous Cell Carcinoma in Mice. *Cancer Lett.* **2008**, *269*, 57–66.
3. Burke, A. R.; Singh, R. N.; Carroll, D. L.; Wood, J. C. S.; D'Agostino, R. B., Jr.; Ajayan, P. M.; Torti, F. M.; Torti, S. V. The Resistance of Breast Cancer Stem Cells to Conventional Hyperthermia and Their Sensitivity to Nanoparticle-Mediated Photothermal Therapy. *Biomaterials* **2012**, *33*, 2961–2970.
4. Pereira, P. L. Actual Role of Radiofrequency Ablation of Liver Metastases. *Eur. Radiol.* **2007**, *17*, 2062–2070.
5. von Maltzahn, G.; Park, J. H.; Agrawal, A.; Bandaru, N. K.; Das, S. K.; Sailor, M. J.; Bhatia, S. N. Computationally Guided Photothermal Tumor Therapy Using Long-Circulating Gold Nanorod Antennas. *Cancer Res.* **2009**, *69*, 3892–3900.
6. Paulet, E.; Aubé, C.; Pessaux, P.; Lebigot, J.; Lhermitte, E.; Oberti, F.; Ponthieux, A.; Calès, P.; Ridereau-Zins, C.; Pereira, P. Factors Limiting Complete Tumor Ablation by Radiofrequency Ablation. *Cardiovasc. Intervent. Radiol.* **2008**, *31*, 107–115.
7. Huang, X.; Jain, P.; El-Sayed, I.; El-Sayed, M. Plasmonic Photothermal Therapy (Pptt) Using Gold Nanoparticles. *Lasers Med. Sci.* **2008**, *23*, 217–228.
8. Hirsch, L. R.; Stafford, R. J.; Bankson, J. A.; Sershen, S. R.; Rivera, B.; Price, R. E.; Hazle, J. D.; Halas, N. J.; West, J. L. Nanoshell-Mediated near-Infrared Thermal Therapy of Tumors under Magnetic Resonance Guidance. *Proc. Natl. Acad. Sci. U.S.A.* **2003**, *100*, 13549–13554.
9. Jain, P. K.; Lee, K. S.; El-Sayed, I. H.; El-Sayed, M. A. Calculated Absorption and Scattering Properties of Gold Nanoparticles of Different Size, Shape, and Composition: Applications in Biological Imaging and Biomedicine. *J. Phys. Chem. B* **2006**, *110*, 7238–7248.
10. Ayala-Orozco, C.; Urban, C.; Knight, M. W.; Urban, A. S.; Neumann, O.; Bishnoi, S. W.; Mukherjee, S.; Goodman, A. M.; Charron, H.; Mitchell, T.; *et al.* Au Nanomatryoshkas as Efficient near-Infrared Photothermal Transducers for Cancer Treatment: Benchmarking against Nanoshells. *ACS Nano* **2014**, *8*, 6372–6381.
11. O'Neal, D. P.; Hirsch, L. R.; Halas, N. J.; Payne, J. D.; West, J. L. Photo-Thermal Tumor Ablation in Mice Using near Infrared-Absorbing Nanoparticles. *Cancer Lett.* **2004**, *209*, 171–176.
12. El-Sayed, M. A.; Shabaka, A. A.; El-Shabrawy, O. A.; Yassin, N. A.; Mahmoud, S. S.; El-Shenawy, S. M.; Al-Ashqar, E.; Eisa, W. H.; Farag, N. M.; El-Shaer, M. A.; *et al.* Tissue Distribution and Efficacy of Gold Nanorods Coupled with Laser Induced Photoplasmonic Therapy in Ehrlich Carcinoma Solid Tumor Model. *PLoS One* **2013**, *8*, e76207.
13. Chithrani, D. B.; Dunne, M.; Stewart, J.; Allen, C.; Jaffray, D. A. Cellular Uptake and Transport of Gold Nanoparticles Incorporated in a Liposomal Carrier. *Nanomed.: Nanotechnol., Biol., Med.* **2010**, *6*, 161–169.
14. Tungjitkusolmun, S.; Staelin, S. T.; Haemmerich, D.; Tsai, J. Z.; Webster, J. G.; Lee, F. T., Jr.; Mahvi, D. M.; Vorperian, V. R. Three-Dimensional Finite-Element Analyses for Radio-Frequency Hepatic Tumor Ablation. *IEEE Trans. Bio-med. Eng.* **2002**, *49*, 3–9.
15. Li, L.; Guan, Y.; Liu, H.; Hao, N.; Liu, T.; Meng, X.; Fu, C.; Li, Y.; Qu, Q.; Zhang, Y.; *et al.* Silica Nanorattle-Doxorubicin-Anchored Mesenchymal Stem Cells for Tumor-Tropic Therapy. *ACS Nano* **2011**, *5*, 7462–7470.
16. Madsen, S. J.; Baek, S. K.; Makkouk, A. R.; Krasieva, T.; Hirschberg, H. Macrophages as Cell-Based Delivery Systems for Nanoshells in Photothermal Therapy. *Ann. Biomed. Eng.* **2012**, *40*, 507–515.
17. Stephan, M. T.; Stephan, S. B.; Bak, P.; Chen, J.; Irvine, D. J. Synapse-Directed Delivery of Immunomodulators Using T-Cell-Conjugated Nanoparticles. *Biomaterials* **2012**, *33*, 5776–5787.
18. Choi, M. R.; Stanton-Maxey, K. J.; Stanley, J. K.; Levin, C. S.; Bardhan, R.; Akin, D.; Badve, S.; Sturgis, J.; Robinson, J. P.; Bashir, R.; *et al.* A Cellular Trojan Horse for Delivery of Therapeutic Nanoparticles into Tumors. *Nano Lett.* **2007**, *7*, 3759–3765.
19. Choi, M. R.; Bardhan, R.; Stanton-Maxey, K. J.; Badve, S.; Nakshatri, H.; Stantz, K. M.; Cao, N.; Halas, N. J.; Clare, S. E. Delivery of Nanoparticles to Brain Metastases of Breast Cancer Using a Cellular Trojan Horse. *Cancer Nanotechnol.* **2012**, *3*, 47–54.
20. Aboody, K. S.; Najbauer, J.; Metz, M. Z.; D'Apuzzo, M.; Gutova, M.; Annala, A. J.; Synold, T. W.; Couture, L. A.; Blanchard, S.; Moats, R. A.; *et al.* Neural Stem Cell–Mediated Enzyme/Prodrug Therapy for Glioma: Preclinical Studies. *Sci. Trans. Med.* **2013**, *5*, 184ra59.
21. Zhao, D.; Najbauer, J.; Annala, A. J.; Garcia, E.; Metz, M. Z.; Gutova, M.; Polewski, M. D.; Gilchrist, M.; Glackin, C. A.; Kim, S. U.; *et al.* Human Neural Stem Cell Tropism to Metastatic Breast Cancer. *Stem Cells* **2012**, *30*, 314–325.
22. Zhao, D.; Najbauer, J.; Garcia, E.; Metz, M. Z.; Gutova, M.; Glackin, C. A.; Kim, S. U.; Aboody, K. S. Neural Stem Cell Tropism to Glioma: Critical Role of Tumor Hypoxia. *Mol. Cancer Res.* **2008**, *6*, 1819–1829.
23. Frank, R. T.; Aboody, K. S.; Najbauer, J. Strategies for Enhancing Antibody Delivery to the Brain. *Biochim. Biophys. Acta* **2011**, *1816*, 191–198.
24. Kim, C. K.; Ahmed, A. U.; Auffinger, B.; Ulasov, I. V.; Tobias, A. L.; Moon, K.-S.; Lesniak, M. S. N-Acetylcysteine Amide Augments the Therapeutic Effect of Neural Stem Cell-Based Antiglioma Oncolytic Virotherapy. *Mol. Ther.* **2013**, *21*, 2063–2073.
25. Ahmed, A. U.; Thaci, B.; Tobias, A. L.; Auffinger, B.; Zhang, L.; Cheng, Y.; Kim, C. K.; Yunis, C.; Han, Y.; Alexiades, N. G.; *et al.* A Preclinical Evaluation of Neural Stem Cell–Based Cell Carrier for Targeted Antiglioma Oncolytic Virotherapy. *J. Natl. Cancer I* **2013**, *105*, 968–977.
26. Ahmed, A. U.; Thaci, B.; Alexiades, N. G.; Han, Y.; Qian, S.; Liu, F.; Balyasnikova, I. V.; Ulasov, I. Y.; Aboody, K. S.; Lesniak, M. S. Neural Stem Cell-Based Cell Carriers Enhance Therapeutic Efficacy of an Oncolytic Adenovirus in an Orthotopic Mouse Model of Human Glioblastoma. *Mol. Ther.* **2011**, *19*, 1714–1726.
27. Cheng, Y.; Morshed, R.; Cheng, S.-H.; Tobias, A.; Auffinger, B.; Wainwright, D. A.; Zhang, L.; Yunis, C.; Han, Y.; Chen, C.-T.; *et al.* Nanoparticle-Programmed Self-Destructive Neural Stem Cells for Glioblastoma Targeting and Therapy. *Small* **2013**, *9*, 4123–4129.
28. Mooney, R.; Weng, Y.; Tirughana-Sambandan, R.; Valenzuela, V.; Aramburo, S.; Garcia, E.; Li, Z.; Gutova, M.; Annala, A. J.; Berlin, J. M.; *et al.* Neural Stem Cells Improve Intracranial Nanoparticle Retention and Tumor-Selective Distribution. *Future Oncol.* **2014**, *10*, 401–415.
29. Mooney, R.; Weng, Y.; Garcia, E.; Bhojane, S.; Smith-Powell, L.; Kim, S. U.; Annala, A. J.; Aboody, K. S.; Berlin, J. M. Conjugation of pH-Responsive Nanoparticles to Neural Stem Cells Improves Intratumoral Therapy. *J. Controlled Release* **2014**, *191*, 82–89.
30. Schnarr, K.; Mooney, R.; Weng, Y.; Zhao, D.; Garcia, E.; Armstrong, B.; Annala, A. J.; Kim, S. U.; Aboody, K. S.; Berlin, J. M. Gold Nanoparticle-Loaded Neural Stem Cells for Photothermal Ablation of Cancer. *Adv. Healthcare Mater.* **2013**, *2*, 976–982.
31. Foulkes, W. D.; Smith, I. E.; Reis-Filho, J. S. Triple-Negative Breast Cancer. *N. Engl. J. Med.* **2010**, *363*, 1938–1948.
32. Chertok, B.; Cole, A. J.; David, A. E.; Yang, V. C. Comparison of Electron Spin Resonance Spectroscopy and Inductively-Coupled Plasma Optical Emission Spectroscopy for Biodistribution Analysis of Iron-Oxide Nanoparticles. *Mol. Pharmaceutics* **2010**, *7*, 375–385.
33. Kim, J. H.; Lee, J. E.; Kim, S. U.; Cho, K. G. Stereological Analysis on Migration of Human Neural Stem Cells in the Brain of Rats Bearing Glioma. *Neurosurgery* **2010**, *66*, 333–342.
34. Chithrani, B. D.; Ghazani, A. A.; Chan, W. C. W. Determining the Size and Shape Dependence of Gold Nanoparticle Uptake into Mammalian Cells. *Nano Lett.* **2006**, *6*, 662–668.

35. Desai, M.; Labhasetwar, V.; Walter, E.; Levy, R.; Amidon, G. The Mechanism of Uptake of Biodegradable Microparticles in Caco-2 Cells Is Size Dependent. *Pharm. Res.* **1997**, *14*, 1568–1573.
36. Zhang, W.; Ji, Y.; Wu, X.; Xu, H. Trafficking of Gold Nanorods in Breast Cancer Cells: Uptake, Lysosome Maturation, and Elimination. *ACS Appl. Mat Interfaces* **2013**, *5*, 9856–9865.
37. Xie, H.; Goins, B.; Bao, A.; Wang, Z. J.; Phillips, W. T. Effect of Intratumoral Administration on Biodistribution of 64cu-Labeled Nanoshells. *Int. J. Nanomed.* **2012**, *7*, 2227–2238.